

# Magnetic-domain-controlled vortex pinning in a superconductor/ferromagnet bilayer

M. Lange, M. J. Van Bael, V. V. Moshchalkov, and Y. Bruynseraede  
*Laboratorium voor Vaste-Stoffysica en Magnetisme,*  
*K. U. Leuven, Celestijnenlaan 200D, B-3001 Leuven, Belgium*  
 (Dated: October 31, 2018)

Vortex pinning in a type-II superconducting Pb film covering a Co/Pt multilayer with perpendicular magnetic anisotropy is investigated. Different stable magnetic domain patterns like band and bubble domains can be created in the Co/Pt multilayer, clearly influencing the vortex pinning in the superconducting Pb layer. Most effective pinning is observed for the bubble domain state. We demonstrate that the pinning properties of the superconductor/ferromagnet bilayer can be controlled by tuning the size, density and magnetization direction of the bubbles.

Magnetic flux penetrates type-II superconductors in the form of quantized vortices, which have the tendency to form a periodic lattice. These vortices move when a current is sent through the superconductor, thus causing dissipation and limiting the critical current density  $j_c$  of the superconductor. To enhance  $j_c$ , vortex motion must be prevented. The latter can be achieved by introducing different pinning centers such as defects created by ion [1] or neutron irradiation [2], lithographically introduced holes [3, 4, 5], or magnetic dots [6, 7, 8, 9].

Recently it was proposed that vortices in a superconductor/ferromagnet (SC/FM) multilayer are strongly pinned if the FM has a stripe domain structure, which typically exists in thin magnetic films with perpendicular anisotropy [10]. Enhanced pinning was observed in SC/FM bilayers compared to SC reference films [11, 12]. However, in these studies the domain structure of the FM was unknown. In this Letter, we systematically investigate the influence of the domains in a ferromagnetic Co/Pt multilayer with perpendicular anisotropy on a *type-II* superconducting Pb film grown on top of the FM. Stable domain structures can be produced in a controlled way by magnetizing the sample before measuring the superconducting properties of the Pb film. We show that the strongest vortex pinning is obtained when localized domains (bubble domains) are present in the FM, and that by changing size and density of the bubbles one can control and optimize the vortex pinning.

The Co/Pt multilayer is deposited on a Si substrate with amorphous SiO<sub>2</sub> top layer in an MBE apparatus by e-beam evaporation. The multilayer has a [Co(0.4 nm)/Pt(1.0 nm)]<sub>10</sub> structure on a 2.8 nm Pt base layer. A 10 nm Ge film, a Pb film with thickness  $d_{Pb} = 50$  nm and a 30 nm Ge capping layer are subsequently evaporated on the Co/Pt multilayer (see Fig. 1) at a substrate temperature of 77 K. The Pb film has a critical temperature of  $T_c = 7.23$  K. The penetration depth  $\lambda(0) = 42$  nm and the coherence length  $\xi(0) = 41$  nm are estimated from measurements of the temperature dependence of the upper critical field. The Ge film between Pb and Co/Pt is insulating at low temperatures, so that the proximity effects between Pb and Co/Pt are suppressed.

The Co/Pt multilayer has perpendicular magnetic anisotropy [13], which is confirmed by hysteresis loop

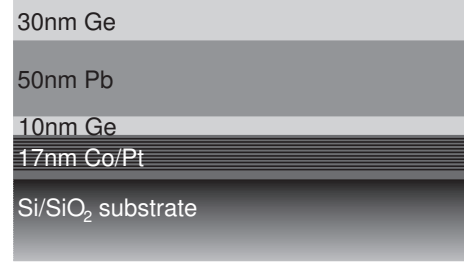


FIG. 1: Schematic presentation of the investigated superconductor/ferromagnet layered structure.

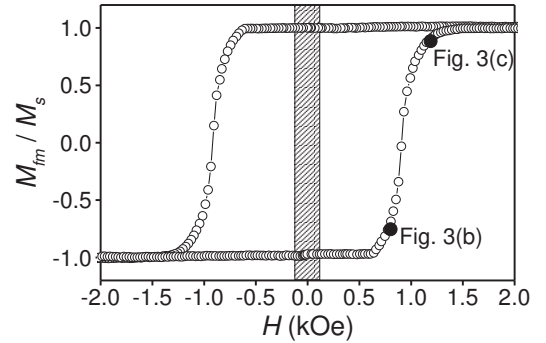


FIG. 2: Hysteresis loop of the Co/Pt multilayer measured by MOKE at room temperature. Magnetic field  $H$  is applied perpendicular to the sample surface. The dashed area shows the field range where magnetization measurements of the superconductor were carried out (Fig. 3).

measurements using the magneto-optical Kerr effect (MOKE). Fig. 2 shows the magnetization  $M_{fm}$  of the Co/Pt multilayer, normalized to the saturation magnetization  $M_s$ , as a function of the magnetic field  $H$  applied perpendicular to the surface. The loop has an almost rectangular shape with  $H_n = 0.6$  kOe,  $H_c = 0.93$  kOe, and  $H_s = 1.45$  kOe, where  $H_n$ ,  $H_c$  and  $H_s$  are the nucleation, coercive and saturation field, respectively.

The microscopic domain structure of the Co/Pt multilayer has been investigated by magnetic force microscopy (MFM) at room temperature and  $H = 0$ . Figs. 3(a)-(c)

show MFM images of the sample in different stable remanent magnetic states. In Fig. 3(a), the sample has been demagnetized by oscillating  $H$  around zero with decreasing amplitude perpendicular to the surface. The dark and bright regions in the image are domains with local magnetic moments  $m$  either pointing up ( $m > 0$ ) or down ( $m < 0$ ), perpendicular to the sample surface. The observed *band domain structure* is typical for Co/Pt multilayers [14]. The width of the band domains is about  $0.2 - 0.4 \mu\text{m}$ .

The images shown in Figs. 3(b) and (c) are obtained after applying a negative field of  $-10 \text{ kOe}$ , sweeping  $H$  to a positive value between  $H_n$  and  $H_s$  as indicated in Fig. 2, and then removing  $H$ . When  $H$  is increased to a value slightly higher than  $H_n$ , small localized domains (bubble domains) with magnetic moments  $m > 0$  nucleate in the film. These bubbles are stable after removing  $H$ , as can be seen in Fig. 3(b). When  $H$  is further increased, the bubbles grow and aggregate. At  $H = H_c$ , there is an equal number of positive and negative  $m$ . If  $H$  is further increased, the number of negative  $m$  decreases and the domains with  $m < 0$  become localized (see Fig. 3(c)). At  $H = H_s$ , the film is saturated with all  $m > 0$ . We introduce the parameter  $s$ , which is defined by the percentage of magnetic moments that are pointing up ( $m > 0$ ), to describe the different remanent magnetic states obtained after this magnetization procedure. For the images shown in Figs. 3(b) and (c),  $s$  is given by the dark area divided by the total area, which is in good agreement with  $s$  calculated from Fig. 2.

The bubble domains in Fig. 3(b) typically have a size of about  $0.35 \mu\text{m}$ , whereas the average size of the bubbles in Fig. 3(c) is about  $0.25 \mu\text{m}$ . Another parameter changing during the reversal process is the number of bubbles per unit area  $\delta$ . For  $H$  only slightly higher than  $H_n$ ,  $\delta$  is very small, but once the bubbles have nucleated in the FM, the reversal process is dominated by domain wall movement and  $\delta$  does not change significantly during this process. From the MFM images, typical values of  $\delta = 1 - 2 \text{ bubbles}/\mu\text{m}^2$  are derived.

After MOKE and MFM measurements, the superconducting Pb film is deposited on the Co/Pt multilayer and the vortex pinning properties are studied by using a Quantum Design SQUID magnetometer. First the FM is brought into a specific magnetic state by applying the same magnetization procedure as for the MFM measurements at 300 K. The magnetization of the FM  $M_{fm}$  is determined from  $M(T)$  data as  $M_{fm} = M(T > T_c)$ , from which the parameter  $s$  of each domain structure is calculated. Repeating the  $M(T)$  measurements in several applied fields ( $|H| < 120 \text{ Oe} \ll H_n$ , see Fig. 2) did not change the value of  $M_{fm}$ , implying that the domain structures are not altered by these small fields. The pinning strength related to each domain structure is determined at 6.9 K by measuring  $M$  as a function of  $H$  applied perpendicular to the surface from  $-120 \text{ Oe}$  to  $+120 \text{ Oe}$ . In order to compare the magnetization curves measured in the different magnetic states,  $M_{fm}$  is sub-

tracted from all curves shown in Fig. 3 (d)-(f), i.e. only the irreversible magnetization of the SC  $M_{sc} = M - M_{fm}$  is plotted. At 6.9 K,  $\xi(6.9\text{K}) = 0.19 \mu\text{m}$  and the effective penetration depth  $\Lambda(6.9\text{K}) = \lambda^2(6.9\text{K})/d_{\text{Pb}} = 0.76 \mu\text{m}$ .

The upper  $M_{sc}(H)$  curve shown in Fig. 3(d) is obtained after demagnetization (corresponding to the MFM image shown in Fig. 3(a)) and the lower one in the  $s = 0$  state, i.e. with the FM fully magnetized in the negative direction. For both magnetic states, a symmetric curve is found. The amplitude of  $M_{sc}(H)$  (which is a measure for the magnitude of  $j_c(H)$  [5]) is lower for all  $H$  when the FM is in the demagnetized state compared to the  $s = 0$  state. This unambiguously shows that the domain structure influences the SC, but does not enhance the vortex pinning in this sample. In the  $s = 0$  state, the stray field of the magnetic film has its largest amplitude at the sample boundary and is much smaller above the center of the FM. This means that the interior of the SC is only weakly influenced by the stray field. Contrary to that, the alternating stray field above the band domains suppresses the order parameter in the SC and may even lead to the creation of vortex-antivortex pairs connecting the domains with opposite magnetization and resulting in a reduction of  $j_c$  [10]. This is also reflected by a decrease of  $T_c$  of the SC to 7.04 K when the band domains are present in the FM.

When bubble domains are present in the FM, the  $M_{sc}(H)$  curve becomes strongly asymmetric with respect to  $H$ . The direction of the asymmetry depends on the mutual orientation of  $H$  and the magnetic moments  $m$  of the bubbles. Fig. 3(e) shows two  $M_{sc}(H)$  curves with  $m$  of the bubbles pointing in the *positive direction* as in Fig. 3(b). Both curves have a larger amplitude of  $M_{sc}$  for positive  $H$ . The upper curve in Fig. 3(f) is obtained after magnetizing the FM in  $H = -20 \text{ kOe} \rightarrow +H_c \rightarrow 0$ , i.e.  $s = 0.5$ .  $M_{sc}(H)$  is almost completely suppressed for this domain state. The other two curves of Fig. 3(f) are obtained with  $m$  of the bubbles in *negative direction* as in Fig. 3(c). Also for this configuration the  $M_{sc}(H)$  curves are asymmetric, but reversed with respect to the field polarity compared to Fig. 3(e).

The asymmetry of  $M_{sc}(H)$  can be explained by a magnetic interaction between vortices and bubble domains. The magnetic interaction can be caused by (i) the interaction between the magnetic field of the vortices  $B$  and the magnetic moments  $m$  in the FM (interaction energy  $E = -mB$ , resulting in attractive interaction for  $m$  and  $B$  having the same polarity, and in repulsive interaction for  $m$  and  $B$  having opposite polarity), and (ii) the interaction between the vortices and the supercurrents generated in the SC by the stray field of the domain structure. During the measurement of  $M_{sc}(H)$  shown in Fig. 3(e), the FM has had bubbles with  $m > 0$ . Hence, evaluating the interaction term  $E = -mB$ , the bubbles act as pinning sites for vortices when  $H > 0$ , resulting in the enhanced amplitude of  $M_{sc}$  for positive  $H$ . Consequently, the bubble domains with  $m < 0$  in Fig. 3(f) are pinning centers for vortices when  $H < 0$ , giving a larger ampli-

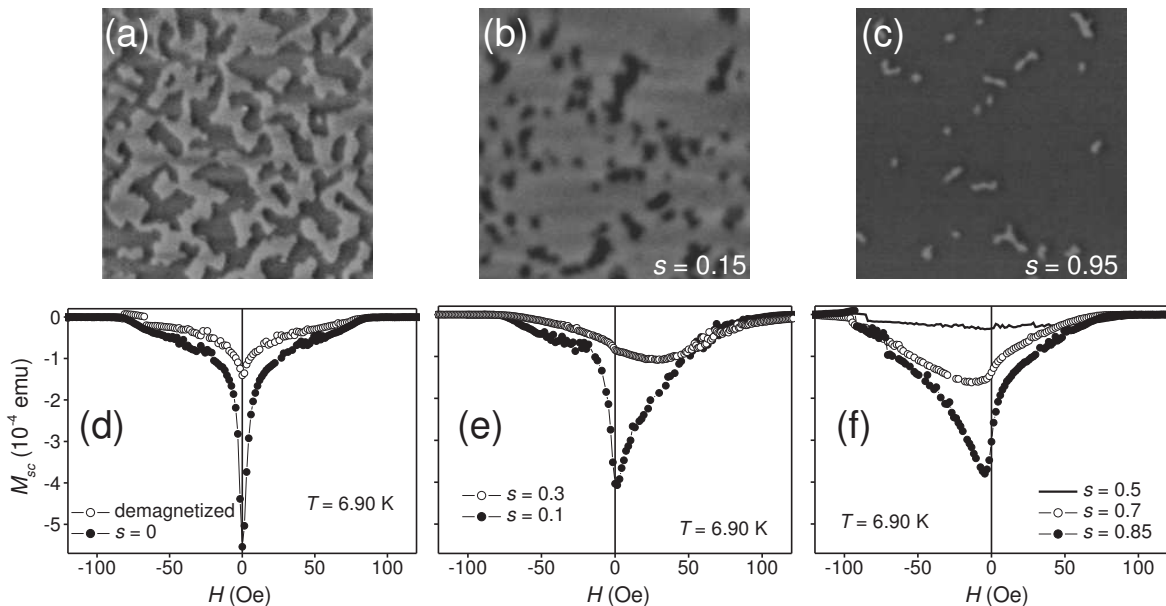


FIG. 3: (a)-(c) MFM images ( $5 \times 5 \mu\text{m}^2$ ) at room temperature and  $H = 0$  of the Co/Pt multilayer in different magnetic states: (a) after demagnetization, (b) after magnetizing the sample in a perpendicularly applied field  $H = -10 \text{ kOe} \rightarrow +0.83 \text{ kOe} \rightarrow 0$  ( $s = 0.15$ ), (c)  $H = -10 \text{ kOe} \rightarrow +1.10 \text{ kOe} \rightarrow 0$  ( $s = 0.95$ ). (d)-(f) Magnetization measurements of a type-II superconducting Pb film covering a Co/Pt multilayer: (d) (○) after demagnetization, (●) in the  $s = 0$  state, (e) (○)  $s = 0.3$ , (●)  $s = 0.1$ , and (f) (○)  $s = 0.5$ , (○)  $s = 0.7$ , (●)  $s = 0.85$ .

tude of  $M_{sc}$  for negative  $H$ . This behavior is consistent with the vortex pinning properties of out-of-plane magnetized dots [8]. Assuming that one bubble can pin one vortex, we can estimate a "matching" field  $H_{match}$  at which all bubbles pin a vortex:  $H_{match} = \phi_0 \delta \approx 20 - 40 \text{ Oe}$ , using  $\delta = 1 - 2/\mu\text{m}^2$  and the flux quantum  $\phi_0$ . In this field range,  $M_{sc}$  indeed has a strongly enhanced amplitude for  $H > 0$  in the  $s = 0.1$  state and for  $H < 0$  in the  $s = 0.85$  state, indicating strong pinning of vortices.

At small fields  $|H| < 3 \text{ Oe}$ ,  $j_c$  is not increased by any of the investigated domain structures compared to the "reference"  $s = 0$  state in which domains are absent. This can be attributed to the stray field above the domains, which results in an overall reduction of the superconducting order parameter  $\psi$ . Figs. 3(e) and (f) also show that more effective vortex pinning is achieved for bubbles with smaller size and lower density. The amplitude of  $M_{sc}$  can be increased up to a factor of 3 when comparing the  $s = 0$  state with the lower curve of Fig. 3(f), and a factor of 2

compared to the middle curve of Fig. 3(f). This indicates that a reduced  $\psi$  associated with bubbles with larger size and higher density counteracts efficient vortex pinning, even leading to the extremely weak amplitude of  $M_{sc}(H)$  for the  $s = 0.5$  state shown in the upper curve of Fig. 3(f).

In conclusion, we have shown that the domain structure in a magnetic film can significantly influence the vortex pinning in a type-II superconductor. By tuning the density of bubble domains in the magnetic film, one can control the vortex pinning. This could be used to design logical devices based on the control of superconductivity by magnetic domain structures [10].

The authors acknowledge L. Van Look, K. Temst and G. Güntherodt for help with sample preparation, and J. Swerts for MOKE measurements. This work was supported by the Belgian IUAP and the Flemish GOA programs, by the ESF "VORTEX" program and by the Fund for Scientific Research (F.W.O.) - Flanders. MJVB is a Postdoctoral Research Fellow of the F.W.O. - Flanders.

[1] L. Civale, A. D. Marwick, T. K., M. A. Kirk, J. R. Thompson, L. Krusinbaum, Y. Sun, J. R. Clem, and F. Holtzberg, Phys. Rev. Lett. **67**, 648 (1991).  
 [2] R. B. vanDover, E. M. Gyorgy, L. F. Schneemeyer, J. W. Mitchell, K. V. Rao, R. Puzniak, and J. V. Waszczak, Nature **342**, 55 (1989).  
 [3] A. T. Fiory, A. F. Hebard, and S. Somekh, Appl. Phys. Lett. **32**, 73 (1978).  
 [4] V. V. Moshchalkov, V. Bruyndoncx, L. Van Look, M. J.

Van Bael, and A. Tonomura, in *Handbook of Nanostructured Materials and Nanotechnology*, edited by H. S. Nalwa (Academic Press, San Diego, 1999), vol. 3, chap. 9, p. 451.  
 [5] V. V. Moshchalkov, M. Baert, V. V. Metlushko, E. Rosseel, M. J. Van Bael, K. Temst, Y. Bruynseraede, and R. Jonckheere, Phys. Rev. B **57**, 3615 (1998).  
 [6] Y. Otani, B. Pannetier, J. P. Nozières, and D. Givord, J. Magn. Magn. Mat. **126**, 622 (1993).

- [7] J. I. Martín, M. Vélez, J. Nogués, and I. K. Schuller, Phys. Rev. Lett. **79**, 1929 (1997).
- [8] D. J. Morgan and J. B. Ketterson, Phys. Rev. Lett. **80**, 3614 (1998).
- [9] M. J. Van Bael, K. Temst, V. V. Moshchalkov, and Y. Bruynseraede, Phys. Rev. B **59**, 14674 (1999).
- [10] L. N. Bulaevskii, E. M. Chudnovsky, and M. P. Maley, Appl. Phys. Lett. **76**, 2594 (2000).
- [11] A. García-Santiago, F. Sánchez, M. Varela, and J. Tejada, Appl. Phys. Lett. **77**, 2900 (2000).
- [12] X. X. Zhang, G. H. Wen, R. K. Zheng, G. C. Xiong, and G. J. Lian, Europhys. Lett. **56**, 119 (2001).
- [13] W. B. Zeper, F. J. A. Greidanus, P. F. Carcia, and C. R. Fincher, J. Appl. Phys. **65**, 4971 (1989).
- [14] M. S. Valera, A. N. Farley, S. R. Hoon, L. Zhou, S. Mcvittie, and J. N. Chapman, Appl. Phys. Lett. **67**, 2566 (1995).